

Low spin wave damping in the insulating chiral magnet Cu_2OSeO_3

I. Stasinopoulos,¹ S. Weichselbaumer,¹ A. Bauer,² J. Waizner,³
H. Berger,⁴ S. Maendl,¹ M. Garst,^{3,5} C. Pfeleiderer,² and D. Grundler^{6,*}

¹*Physik Department E10, Technische Universität München, D-85748 Garching, Germany*

²*Physik Department E51, Technische Universität München, D-85748 Garching, Germany*

³*Institute for Theoretical Physics, Universität zu Köln, D-50937 Köln, Germany*

⁴*Institut de Physique de la Matière Complexe, École Polytechnique Fédérale de Lausanne, 1015 Lausanne, Switzerland*

⁵*Institut für Theoretische Physik, Technische Universität Dresden, D-01062 Dresden, Germany*

⁶*Institute of Materials and Laboratory of Nanoscale Magnetic Materials and Magnonics (LMGN),
École Polytechnique Fédérale de Lausanne (EPFL), Station 12, 1015 Lausanne, Switzerland*

(Dated: March 7, 2024)

Chiral magnets with topologically nontrivial spin order such as Skyrmions have generated enormous interest in both fundamental and applied sciences. We report broadband microwave spectroscopy performed on the insulating chiral ferrimagnet Cu_2OSeO_3 . For the damping of magnetization dynamics we find a remarkably small Gilbert damping parameter of about 1×10^{-4} at 5 K. This value is only a factor of 4 larger than the one reported for the best insulating ferrimagnet yttrium iron garnet. We detect a series of sharp resonances and attribute them to confined spin waves in the mm-sized samples. Considering the small damping, insulating chiral magnets turn out to be promising candidates when exploring non-collinear spin structures for high frequency applications.

PACS numbers: 76.50.+g, 74.25.Ha, 4.40.Az, 41.20.Jb

The development of future devices for microwave applications, spintronics and magnonics [1–3] requires materials with a low spin wave (magnon) damping. Insulating compounds are advantageous over metals for high-frequency applications as they avoid damping via spin wave scattering at free charge carriers and eddy currents [4, 5]. Indeed, the ferrimagnetic insulator yttrium iron garnet (YIG) holds the benchmark with a Gilbert damping parameter $\alpha_{\text{intr}} = 3 \times 10^{-5}$ at room temperature [6, 7]. During the last years chiral magnets have attracted a lot of attention in fundamental research and stimulated new concepts for information technology [8, 9]. This material class hosts non-collinear spin structures such as spin helices and Skyrmions below the critical temperature T_c and critical field H_{c2} [10–12]. Additionally, Dzyaloshinskii-Moriya interaction (DMI) is present that induces both the Skyrmion lattice phase and nonreciprocal microwave characteristics [13]. Low damping magnets offering DMI would generate new prospects by particularly combining complex spin order with long-distance magnon transport in high-frequency applications and magnonics [14, 15]. At low temperatures, they would further enrich the physics in magnon-photon cavities that call for materials with small α_{intr} to achieve high-cooperative magnon-to-photon coupling in the quantum limit [16–19].

In this work, we investigate the Gilbert damping in Cu_2OSeO_3 , a prototypical insulator hosting Skyrmions [20–23]. This material is a local-moment ferrimagnet with $T_c = 58$ K and magnetoelectric coupling [24] that gives rise to dichroism for microwaves [25–27]. The magnetization dynamics in Cu_2OSeO_3 has already been explored [13, 28, 29]. A detailed investigation on the

damping which is a key quality for magnonics and spintronics has not yet been presented however. To evaluate α_{intr} we explore the field polarized state (FP) where the two spin sublattices attain the ferrimagnetic arrangement [21]. Using spectra obtained by two different coplanar waveguides (CPWs), we extract a minimum $\alpha_{\text{intr}} = (9.9 \pm 4.1) \times 10^{-5}$ at 5 K, i.e. only about four times higher than in YIG. We resolve numerous sharp resonances in our spectra and attribute them to modes that are confined modes across the macroscopic sample and allowed for by the low damping. Our findings substantiate the relevance of insulating chiral magnets for future applications in magnonics and spintronics.

From single crystals of Cu_2OSeO_3 we prepared two bar-shaped samples exhibiting different crystallographic orientations. The samples had lateral dimensions of $2.3 \times 0.4 \times 0.3$ mm³. They were positioned on CPWs that provided us with a dynamic magnetic field \mathbf{h} induced by a sinusoidal current applied to the signal surrounded by two ground lines. We used two different CPWs with either a broad [30] or narrow signal line width of $w_s = 1$ mm or $20 \mu\text{m}$, respectively [31]. The central long axis of the rectangular Cu_2OSeO_3 rods was positioned on the central axis of the CPWs. The static magnetic field \mathbf{H} was applied perpendicular to the substrate with $\mathbf{H} \parallel \langle 100 \rangle$ and $\mathbf{H} \parallel \langle 111 \rangle$ for sample S1 and S2, respectively. The direction of H defined the z -direction. The dynamic field component $\mathbf{h} \perp \mathbf{H}$ provided the relevant torque for excitation. Components $\mathbf{h} \parallel \mathbf{H}$ did not induce precessional motion in the FP state of Cu_2OSeO_3 . We recorded spectra by a vector network analyzer using the magnitude of the scattering parameter S_{12} . We subtracted a background spectrum recorded at 1 T to enhance the signal-to-noise

ratio (SNR) yielding the displayed $\Delta|S_{12}|$. In Ref. [7], Klingler *et al.* have investigated the damping of the insulating ferrimagnet YIG and found that Gilbert parameters α_{intr} evaluated from both the uniform precessional mode and standing spin waves confined in the macroscopic sample provided the same values. For Cu_2OSeO_3 we evaluated α in two ways [32]. When extracting the linewidth ΔH for different resonance frequencies f_r , the Gilbert damping parameter α_{intr} was assumed to vary according to [33, 34]

$$\mu_0\gamma \cdot \Delta H = 4\pi\alpha_{\text{intr}} \cdot f_r + \mu_0\gamma \cdot \Delta H_0, \quad (1)$$

where γ is the gyromagnetic factor and ΔH_0 the contribution due to inhomogeneous broadening. Equation (1) is valid when viscous Gilbert damping dominates over scattering within the magnetic subsystem [35]. When performing frequency-swept measurements at different fields H , the obtained linewidth Δf was considered to scale linearly with the resonance frequency as [36]

$$\Delta f = 2\alpha_{\text{intr}} \cdot f_r + \Delta f_0, \quad (2)$$

with the inhomogeneous broadening Δf_0 . The conversion from Eq. (1) to Eq. (2) is valid when f_r scales linearly with H and \mathbf{H} is applied along a magnetic easy or hard axis of the material [37, 38]. In Fig. 1 (a) to (d) we show spectra recorded in the FP state of the material using the two different CPWs. For the same applied field H we observe peaks residing at higher frequency f for $\mathbf{H} \parallel \langle 100 \rangle$ compared to $\mathbf{H} \parallel \langle 111 \rangle$. From the resonance frequencies, we extract the cubic magnetocrystalline anisotropy constant $K = (-0.6 \pm 0.1) \cdot 10^3 \text{ J/m}^3$ for Cu_2OSeO_3 [31]. The magnetic anisotropy energy is found to be extremal for $\langle 100 \rangle$ and $\langle 111 \rangle$ reflecting easy and hard axes, respectively [31]. The saturation magnetization of Cu_2OSeO_3 amounted to $\mu_0 M_s = 0.13 \text{ T}$ at 5 K [22].

Figure 1 summarizes spectra taken with two different CPWs on two different Cu_2OSeO_3 crystals exhibiting different crystallographic orientation in the field H . For the narrow CPW [Fig. 1 (a) and (c)], we observed a broad peak superimposed by a series of resonances that all shifted to higher frequencies with increasing H . The field dependence excluded them from being noise or artifacts of the setup. Their number and relative intensities varied from sample to sample and also upon remounting the same sample in the cryostat (not shown). They disappeared with increasing temperature T but the broad peak remained. For the broad CPW [Fig. 1 (b) and (d)], we measured pronounced peaks whose linewidths were significantly smaller compared to the broad peak detected with the narrow CPW. We resolved resonances below the large peaks [arrows in Fig. 1 (b)] that shifted with H and exhibited an almost field-independent frequency offset from the main peaks that we will discuss later. It is instructive to first follow the orthodox approach and analyze damping parameters from modes reflecting the

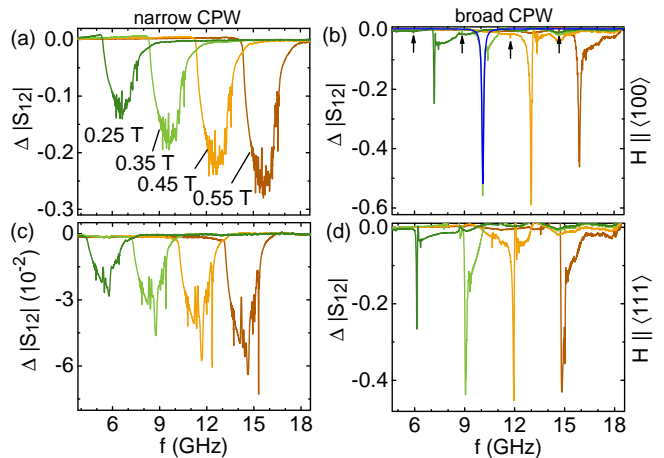


FIG. 1. (Color online) Spectra $\Delta|S_{12}|$ obtained at $T = 5 \text{ K}$ for different \mathbf{H} using (a) a narrow and (b) broad CPW when $\mathbf{H} \parallel \langle 100 \rangle$ on sample S1. Corresponding spectra taken on sample S2 for $\mathbf{H} \parallel \langle 111 \rangle$ are shown in (c) and (d), respectively. Note the strong and sharp resonances in (b) and (d) when using the broad CPW that provides a much more homogeneous excitation field \mathbf{h} . Arrows mark resonances that have a field-independent offset with the corresponding main peaks and are attributed to standing spin waves. An exemplary Lorentz fit curve is shown in blue color in (b).

excitation characteristics of the CPW [29]. Second, we follow Ref. [7] and analyze confined modes.

Lorentz curves (blue) were fitted to the spectra recorded with the broad CPW to determine resonance frequencies and linewidths. Note that the corresponding linewidths were larger by a factor of $\sqrt{3}$ compared to the linewidth Δf that is conventionally extracted from the imaginary part of the scattering parameters [39]. The extracted linewidths Δf were found to follow linear fits based on Eq. (2) at different temperatures (details are shown in Ref. [31]). In Fig. 2 (a) we show a resonance curve that was obtained as a function of H taken with the narrow CPW at 15 GHz. The curve does not show sharp features as H was varied in finite steps (symbols). The linewidth ΔH (symbols) is plotted in Fig. 2 (b) for different resonance frequencies and temperatures. The data are well described by linear fits (lines) based on Eq. (1). Note that the resonance peaks measured with the broad CPW were extremely sharp. The sharpness did not allow us to analyze the resonances as a function of H . We refrained from fitting the broad peaks of Fig. 1 (a) and (c) (narrow CPW) as they showed a clear asymmetry attributed to the overlap of subresonances at finite wavevector k , as will be discussed below.

In Fig. 3 (a) and (b) we compare the parameter α_{intr} obtained from both different CPWs (circles vs. stars) and the two evaluation routes [40]. For $\mathbf{H} \parallel \langle 100 \rangle$ [Fig. 3 (a)], between 5 and 20 K the lowest value for α_{intr} amounts to $(3.7 \pm 0.4) \times 10^{-3}$. This value is three times lower compared to preliminary data presented in Ref. [29]. Beyond

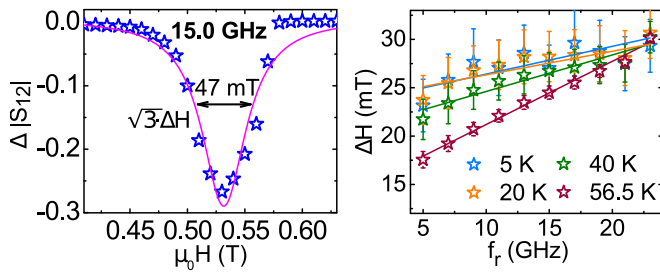


FIG. 2. (Color online) (a) Lorentz curve (magenta line) fitted to a resonance (symbols) measured at $f = 15$ GHz as a function of H at 5 K. (b) Frequency dependencies of linewidths ΔH (symbols) for four different T . We performed the $\sqrt{3}$ -correction. The slopes of linear fits (straight lines) following Eq. 1 are considered to reflect the intrinsic damping parameters α_{intr} .

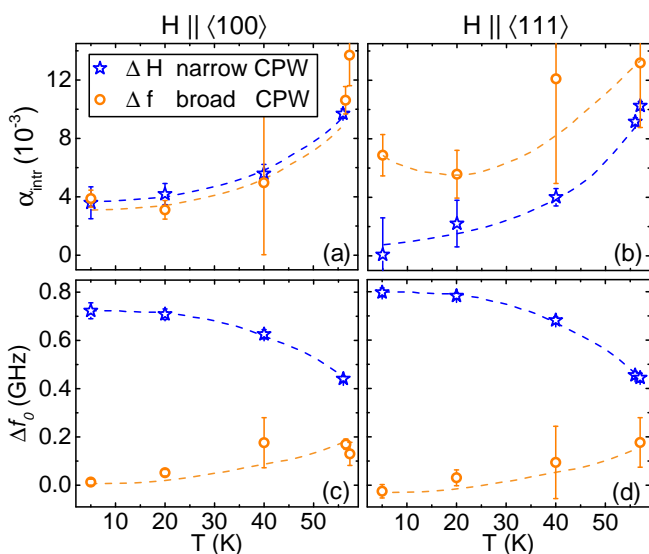


FIG. 3. (Color online) (a) and (b) Intrinsic damping parameters α_{intr} and inhomogeneous broadening Δf_0 for two different field directions (see labels) obtained from the slopes and intercepts at $f_r = 0$ of linear fits to the linewidth data (see Fig. 2 (b) and Ref. [31]). Dashed lines are guides to the eyes.

20 K the damping is found to increase. For $\mathbf{H} \parallel \langle 111 \rangle$ [Fig. 3 (b)] we extract $(0.6 \pm 0.6) \times 10^{-3}$ as the smallest value. Note that these values for α_{intr} still contain an extrinsic contribution and thus represent upper bounds for Cu_2OSeO_3 , as we will show later. For the inhomogeneous broadening Δf_0 in Fig. 3 (c) and (d) the datasets are consistent (we have used the relation $\Delta f_0 = \gamma \Delta H_0 / 2\pi$ to convert ΔH_0 into Δf_0). We see that Δf_0 increases with T and is small for the broad CPW, independent of the crystallographic direction of H . For the narrow CPW the inhomogeneous broadening is largest at small T and then decreases by about 40 % up to about 50 K. Note that a CPW broader than the sample is assumed to excite homogeneously at f_{FMR} [41] transferring a wave vector $k = 0$ to the sample. Accordingly

we ascribe the intense resonances of Fig. 1 (b) and (d) to f_{FMR} . Using $f_{\text{FMR}} = 6$ GHz and $\alpha_{\text{intr}} = 3.7 \times 10^{-3}$ at 5 K [Fig. 3 (a)], we estimate a minimum relaxation time of $\tau = [2\pi\alpha_{\text{intr}}f_r]^{-1} = 6.6$ ns.

In the following, we examine in detail the additional sharp resonances that we observed in spectra of Fig. 1. In Fig. 1 (b) taken with the broad CPW for $\mathbf{H} \parallel \langle 100 \rangle$, we identify sharp resonances that exhibit a characteristic frequency offset δf with the main resonance at all fields (black arrows). We illustrate this in Fig. 4(a) in that we shift spectra of Fig. 1 (b) so that the positions of their main resonances overlap. The additional small resonances (arrows) in Fig. 1 (b) are well below the uniform mode. This is characteristic for backward volume magnetostatic spin waves (BVMSWs). Standing waves of such kind can develop if they are reflected at least once at the bottom and top surfaces of the sample. The resulting standing waves exhibit a wave vector $k = n\pi/d$, with order number n and sample thickness $d = 0.3$ mm. The BVMSW dispersion relation $f(k)$ of Ref. [13] provides a group velocity $v_g = -300$ km/s at $k = \pi/d$ [triangles in Fig. 4 (b)]. Hence, the decay length $l_d = v_g\tau$ amounts to 2 mm considering $\tau = 6.6$ ns. This is larger than twice the relevant lateral sizes, thereby allowing standing spin wave modes to form in the sample. Based on the dispersion relation of Ref. [13], we calculated the frequency splitting $\delta f = f_{\text{FMR}} - f(n\pi/d)$ [open diamonds in Fig. 4 (b)] assuming $n = 1$ and $t = 0.4$ mm for the sample width t defined in Ref. [13]. Experimental values (filled symbols) agree with the calculated ones (open symbols) within about 60 MHz. In case of the narrow CPW, we observe even more sharp resonances [Fig. 1 (a) and (c)]. A set of resonances was reported previously in the field-polarized phase of Cu_2OSeO_3 [26, 28, 42, 43]. Maisuradze *et al.* assigned secondary peaks in thin plates of Cu_2OSeO_3 to different standing spin-wave modes [43] in agreement with our analysis outlined above.

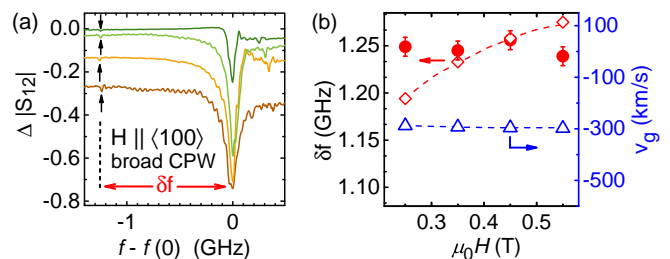


FIG. 4. (Color online) (a) Spectra of Fig. 1 (b) replotted as $f - f_{\text{FMR}}(H)$ for different H such that all main peaks are at zero frequency and the field-independent frequency splitting δf becomes visible. The numerous oscillations seen particularly on the bottom most curve are artefacts from the calibration routine. (b) Experimentally evaluated (filled circles) and theoretically predicted (diamonds) splitting δf using dispersion relations for a platelet. Calculated group velocity v_g at $k = \pi/(0.3 \text{ mm})$. Dashed lines are guides to the eyes.

The inhomogeneous dynamic field \mathbf{h} of the narrow CPW provides a much broader distribution of \mathbf{k} compared to the broad CPW. This is consistent with the fact that the inhomogeneous broadening Δf_0 is found to be larger for the narrow CPW compared to the broad one [Fig. 3 (c) and (c)]. Under these circumstances, the excitation of more standing waves is expected. We attribute the series of sharp resonances in Fig. 1 (a) and (c) to such spin waves. In Fig. 5 (a) and (b) we highlight prominent and particularly narrow resonances with #1, #2 and #3 recorded with the narrow CPW. We trace their frequencies f_r as a function of H for $\mathbf{H} \parallel \langle 100 \rangle$ and $\mathbf{H} \parallel \langle 111 \rangle$, respectively. They depend linearly on H suggesting a Landé factor $g = 2.14$ at 5 K.

We now concentrate on mode #1 for $\mathbf{H} \parallel \langle 100 \rangle$ at 5 K that is best resolved. We fit a Lorentzian line-shape as shown in Fig. 5(c) for 0.85 T, and summarize the corresponding linewidths Δf in Fig. 5(d). The inset of Fig. 5(d) shows the effective damping $\alpha_{\text{eff}} = \Delta f / (2f_r)$ evaluated directly from the linewidth as suggested in Ref. [29]. We find that α_{eff} approaches a value of about 3.5×10^{-4} with increasing frequency. This value includes both the intrinsic damping and inhomogeneous broadening but is already a factor of 10 smaller compared to α_{intr} extracted from Fig. 3 (a). Note that Cu_2OSeO_3 exhibiting 3.5×10^{-4} outperforms the best metallic thin-film magnet [44]. To correct for inhomogeneous broadening and determine the intrinsic Gilbert-type damping, we apply a linear fit to the linewidths Δf in Fig. 5(d) at $f_r > 10.6$ GHz and obtain $(9.9 \pm 4.1) \times 10^{-5}$. For $f_r \leq 10.6$ GHz the resonance amplitudes of mode #1 were small reducing the confidence of the fitting procedure. Furthermore, at low frequencies, we expect anisotropy to modify the extracted damping, similar to the results in Ref. [45]. For these reasons, the two points at low f_r were left out for the linear fit providing $(9.9 \pm 4.1) \times 10^{-5}$.

We find Δf and the damping parameters of Fig. 3 to increase with T . It does not scale linearly for $\mathbf{H} \parallel \langle 100 \rangle$ [31]. A deviation from linear scaling was reported for YIG single crystals as well and accounted for by the confluence of a low- k magnon with a phonon or thermally excited magnon [5]. In the case of $\mathbf{H} \parallel \langle 111 \rangle$ (cf. Fig. 3 (b)) we obtain a clear discrepancy between results from the two evaluation routes and CPWs used. We relate this observation to a misalignment of \mathbf{H} with the hard axis $\langle 111 \rangle$. The misalignment motivates a field-dragging contribution [38] that can explain the discrepancy. For this reason, we concentrated our standing wave analysis on the case $\mathbf{H} \parallel \langle 100 \rangle$. We now comment on our spectra taken with the broad CPW that do not show the very small linewidth attributed to the confined spin waves. The sharp mode #1 yields $\Delta f = 15.3$ MHz near 16 GHz [Fig. 5 (d)]. At 5 K the dominant peak measured at 0.55 T with the broad CPW provides however $\Delta f = 129$ MHz. Δf obtained by the broad CPW is thus increased by a factor of eight and explains the relatively large Gilbert

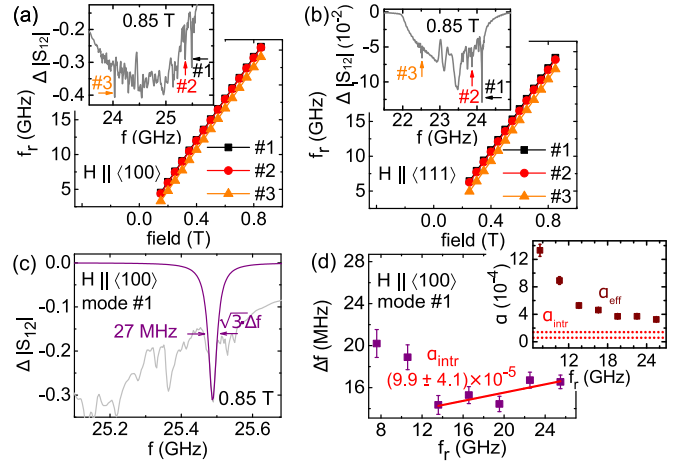


FIG. 5. (Color online) (a)-(b) Resonance frequency as a function of field H of selected sharp modes labelled #1 to #3 (see insets) for $\mathbf{H} \parallel \langle 100 \rangle$ and $\mathbf{H} \parallel \langle 111 \rangle$ at $T = 5$ K. (c) Exemplary Lorentz fit of sharp mode #1 for $\mathbf{H} \parallel \langle 100 \rangle$ at 0.85 T. (d) Extracted linewidth Δf as a function of resonance frequency f_r along with the linear fit performed to determine the intrinsic damping α_{intr} in Cu_2OSeO_3 . Inset: Comparison among the extrinsic and intrinsic damping contribution. The red dotted lines mark the error margins of $\alpha_{\text{intr}} = (9.9 \pm 4.1) \times 10^{-5}$.

damping parameter in Fig. 3 (a) and (b). We confirmed this larger value on a third sample with $\mathbf{H} \parallel \langle 100 \rangle$ and obtained $(3.1 \pm 0.3) \times 10^{-3}$ [31] using the broad CPW. The discrepancy with the damping parameter extracted from the sharp modes of Fig. 5 might be due to the remaining inhomogeneity of \mathbf{h} over the thickness of the sample leading to an uncertainty in the wave vector in z -direction. For a standing spin wave such an inhomogeneity does not play a role as the boundary conditions discretize k . Accordingly, Klingler *et al.* extract the smallest damping parameter of $2.7(5) \times 10^{-5}$ reported so far for the ferrimagnet YIG when analyzing confined magnetostatic modes [7].

To summarize, we investigated the spin dynamics in the field-polarized phase of the insulating chiral magnet Cu_2OSeO_3 . We detected numerous sharp resonances that we attribute to standing spin waves. Their effective damping parameter is small and amounts to 3.5×10^{-4} . A quantitative estimate of the intrinsic Gilbert damping parameter extracted from the confined modes provides even $\alpha_{\text{intr}} = (9.9 \pm 4.1) \times 10^{-5}$ at 5 K. The small damping makes an insulating ferrimagnet exhibiting Dzyaloshinskii-Moriya interaction a promising candidate for exploitation of complex spin structures and related nonreciprocity in magnonics and spintronics.

We thank S. Mayr for assistance with sample preparation. Financial support through DFG TRR80, DFG 1143, DFG FOR960, and ERC Advanced Grant 291079 (TOPFIT) is gratefully acknowledged.

-
- * Electronic mail: dirk.grundler@epfl.ch
- [1] I. Zutic and H. Dery, *Nat. Mater.* **10**, 647 (2011).
 - [2] M. Krawczyk and D. Grundler, *J. Phys.: Condens. Matter* **26**, 123202 (2014).
 - [3] A. V. Chumak, V. I. Vasyuchka, A. A. Serga, and B. Hillebrands, *Nat. Phys.* **11**, 453 (2015).
 - [4] A. G. Gurevich and G. A. Melkov, *Magnetization Oscillations and Waves* (CRC Press, 1996).
 - [5] M. Sparks, *Ferromagnetic-Relaxation Theory* (McGraw-Hill, 1964).
 - [6] A. A. Serga, A. V. Chumak, and B. Hillebrands, *Journal of Physics D: Applied Physics* **43**, 264002 (2010).
 - [7] S. Klingler, H. Maier-Flaig, C. Dubs, O. Surzhenko, R. Gross, H. Huebl, S. T. B. Goennenwein, and M. Weiler, *Applied Physics Letters* **110**, 092409 (2017), <http://dx.doi.org/10.1063/1.4977423>.
 - [8] A. Fert, V. Cros, and J. Sampaio, *Nat. Nanotechn.* **8**, 152 (2013).
 - [9] N. Nagaosa and Y. Tokura, *Nat. Nanotechn.* **8**, 899 (2013).
 - [10] S. Mühlbauer, B. Binz, F. Jonietz, C. Pfleiderer, A. Rosch, A. Neubauer, R. Georgii, and P. Böni, *Science* **323**, 915 (2009).
 - [11] X. Z. Yu, Y. Onose, N. Kanazawa, J. H. Park, J. H. Han, Y. Matsui, N. Nagaosa, and Y. Tokura, *Nature (London)* **465**, 901 (2010).
 - [12] S. Seki, X. Z. Yu, S. Ishiwata, and Y. Tokura, *Science* **336**, 198 (2012).
 - [13] S. Seki, Y. Okamura, K. Kondou, K. Shibata, M. Kubota, R. Takagi, F. Kagawa, M. Kawasaki, G. Tatara, Y. Otani, and Y. Tokura, *Phys. Rev. B* **93**, 235131 (2016).
 - [14] M. Mochizuki and S. Seki, *J. Physics: Condens. Matter* **27**, 503001 (2015).
 - [15] M. Garst, J. Waizner, and D. Grundler, <https://arxiv.org/abs/1702.03668> (2017).
 - [16] H. Huebl, C. W. Zollitsch, J. Lotze, F. Hocke, M. Greifenstein, A. Marx, R. Gross, and S. T. B. Goennenwein, *Phys. Rev. Lett.* **111**, 127003 (2013).
 - [17] Y. Tabuchi, S. Ishino, T. Ishikawa, R. Yamazaki, K. Usami, and Y. Nakamura, *Phys. Rev. Lett.* **113**, 083603 (2014).
 - [18] X. Zhang, C.-L. Zou, L. Jiang, and H. X. Tang, *Phys. Rev. Lett.* **113**, 156401 (2014).
 - [19] M. Goryachev, W. G. Farr, D. L. Creedon, Y. Fan, M. Kostylev, and M. E. Tobar, *Phys. Rev. Applied* **2**, 054002 (2014).
 - [20] K. Kohn, *J. Phys. Soc. Jpn* **42**, 2065 (1977).
 - [21] M. Belesi, I. Rousochatzakis, H. C. Wu, H. Berger, I. V. Shvets, F. Mila, and J. P. Ansermet, *Phys. Rev. B* **82**, 094422 (2010).
 - [22] T. Adams, A. Chacon, M. Wagner, A. Bauer, G. Brandl, B. Pedersen, H. Berger, P. Lemmens, and C. Pfleiderer, *Phys. Rev. Lett.* **108**, 237204 (2012).
 - [23] S. Seki, J.-H. Kim, D. S. Inosov, R. Georgii, B. Keimer, S. Ishiwata, and Y. Tokura, *Phys. Rev. B* **85**, 220406 (R) (2012).
 - [24] S. Seki, S. Ishiwata, and Y. Tokura, *Phys. Rev. B* **86**, 060403 (2012).
 - [25] Y. Okamura, F. Kagawa, M. Mochizuki, M. Kubota, S. Seki, S. Ishiwata, M. Kawasaki, Y. Onose, and Y. Tokura, *Nat. Commun.* **4**, 2391 (2013).
 - [26] Y. Okamura, F. Kagawa, S. Seki, M. Kubota, M. Kawasaki, and Y. Tokura, *Phys. Rev. Lett.* **114**, 197202 (2015).
 - [27] M. Mochizuki, *Phys. Rev. Lett.* **114**, 197203 (2015).
 - [28] Y. Onose, Y. Okamura, S. Seki, S. Ishiwata, and Y. Tokura, *Phys. Rev. Lett.* **109**, 037603 (2012).
 - [29] T. Schwarze, J. Waizner, M. Garst, A. Bauer, I. Stasinopoulos, H. Berger, C. Pfleiderer, and D. Grundler, *Nature Mater.* **14**, 478 (2015).
 - [30] Model B4350-30C from Southwest Microwave, Inc., www.southwestmicrowave.com.
 - [31] See Supplemental Material at [URL] for experimental details and additional data.
 - [32] Y. Wei, S. L. Chin, and P. Svedlindh, *J. Phys. D: Appl. Phys.* **48**, 335005 (2015).
 - [33] B. Heinrich, J. F. Cochran, and R. Hasegawa, *J. Appl. Phys.* **57** (1985).
 - [34] S. S. Kalarickal, P. Krivosik, M. Wu, C. E. Patton, M. L. Schneider, P. Kabos, T. J. Silva, and J. P. Nibarger, *J. Appl. Phys.* **99**, 093909 (2006).
 - [35] K. Lenz, H. Wende, W. Kuch, K. Baberschke, K. Nagy, and A. Jánosy, *Phys. Rev. B* **73**, 144424 (2006).
 - [36] C. E. Patton, *J. Appl. Phys.* **39** (1968).
 - [37] B. Kuanr, R. E. Camley, and Z. Celinski, *Appl. Phys. Lett.* **87**, 012502 (2005).
 - [38] M. Farle and H. Zabel, *Magnetic Nanostructures Spin Dynamics and Spin Transport*, Vol. 246 (Springer Tracts in Modern Physics, 2013).
 - [39] D. D. Stancil and A. Prabhakar, *Spin Waves Theory and Applications* (Springer, 2009).
 - [40] We call it α_{intr} at this point as the parameter is extracted from linear slopes. Later we will show that standing spin waves provide the lowest α_{intr} .
 - [41] Y. Iguchi, S. Uemura, K. Ueno, and Y. Onose, *Phys. Rev. B* **92**, 184419 (2015).
 - [42] M. I. Kobets, K. G. Dergachev, E. N. Khatsko, A. I. Rykova, P. Lemmens, D. Wulferding, and H. Berger, *Low Temp. Phys.* **36** (2010).
 - [43] A. Maisuradze, A. Shengelaya, H. Berger, D. M. Djokić, and H. Keller, *Phys. Rev. Lett.* **108**, 247211 (2012).
 - [44] M. A. W. Schoen, D. Thonig, M. L. Schneider, T. J. Silva, H. T. Nembach, O. Eriksson, O. Karis, and J. M. Shaw, *Nat. Phys.* **12**, 839 (2016).
 - [45] T. J. Silva, C. S. Lee, T. M. Crawford, and C. T. Rogers, *J. Appl. Phys.* **85** (1999).